C. R. Geoscience 351 (2019) 37–47

Contents lists available at ScienceDirect

Comptes Rendus Geoscience

www.sciencedirect.com

Hydrology, Environment (Surface Geochemistry)

Phosphate removal from water by naturally occurring shale, sandstone, and laterite: The role of iron oxides and of soluble species

Dan Eude Kpannieu [a,b], Martine Mallet [a], Lacina Coulibaly [b], Mustapha Abdelmoula [a], Christian Ruby [a,*]

[a] Laboratoire de chimie physique et microbiologie pour les matériaux et l'environnement, LCPME, UMR 7564 CNRS, Université de Lorraine, 405, rue de Vandœuvre, 54600 Villers-lès-Nancy, France
[b] Laboratoire d'environnement et biologie aquatique, Université Nangui-Abrogoua, 02 BP 801, Abidjan 02, Cote d'Ivoire

ARTICLE INFO

Article history:
Received 17 September 2018
Accepted after revision 25 September 2018
Available online 16 November 2018

Handled by François Chabaux

Keywords:
Phosphate
Adsorption
Iron
Geomaterials
Ivory Coast

ABSTRACT

Aqueous phosphate removal by three geomaterials from Ivory Coast was evaluated to determine their potential application as low-cost phosphate adsorbents in wastewater treatment. Batch experiments showed that phosphate uptake strongly depended on pH. Laterite and sandstone dissolution was less pronounced compared to shale. A correlation between concentrations of aqueous cation species released from shale and phosphate uptake was observed. The kinetics were well described using the pseudo-second-order model. Isotherms displayed a saturation level on shale, while phosphate uptake continuously increased for laterite and sandstone. The removal efficiency decreased in the following ranking order: laterite > sandstone > shale. Laterite was also the most efficient adsorbent in column experiments. The high phosphate removal efficiency of laterite (8.3 mg PO_4 g^{-1}) was attributed to the presence of superparamagnetic low grain sizes of goethite. Laterite is a particularly promising material for further investigation in wastewater treatment technology such as constructed wetlands.

1. Introduction

Phosphorous is an essential nutrient for the growth of aquatic plants and algae, but its excessive supply in water bodies causes eutrophication resulting in increased growth of algae, depletion of oxygen, and disruption in the balance of organisms. Excessive phosphate input to waters originates from anthropogenic activities such as wastewater discharges and agricultural run-off. In wastewater treatment technology, chemical and biological removal techniques are the most effective and well-established methods, but their high cost and complexity of implementation prevent their application both in rural areas and in developing countries. Recently, attention has been focused on developing alternative methods for phosphate removal from water. Among these methods, adsorption appears as an attractive option, owing to its low cost and easy application (Boyer et al., 2011; Hongbin and Ming, 2014). A large variety of materials with the availability to remove phosphate were thus described in the literature (Johansson-Westholm, 2006; Vohla et al., 2011; Wendling et al., 2013). High sorption capacity, low cost, availability in large quantity and environmentally-friendly nature are among the most important parameters in the choice of the

* Corresponding author.
E-mail address: Christian.ruby@univ-lorraine.fr (C. Ruby).

https://doi.org/10.1016/j.crte.2018.09.004

sorbent. The present paper reports a study that aimed to develop a material satisfying all these criteria with the final objective of applying this optimized material in the treatment of wastewaters released into the Ebrié lagoon in Ivory Coast. In fact, the eutrophication of the Ebrié lagoon is dramatic in large areas, making the lagoon actually unsafe for habitation sites, for the practice of lucrative activities such as bathing and fishing (Briton et al., 2007; Koffi et al., 2009; Tuo et al., 2012; Yao et al., 2009). Interestingly, shale, sandstone and laterite are low cost and environmentally friendly geological materials easily available in large quantities in Ivory Coast. In addition to this context, these geomaterials are expected to contain separate iron oxide minerals and/or iron in structural substitution and are thus expected to be promising phosphate adsorbents.

The main objective of the present paper is to study the sorption behavior of phosphate onto three natural, available and inexpensive geomaterials from Ivory Coast to determine the best candidate for a further application in a micro-pilot unit and ultimately in a wetland system. Batch sorption experiments were carried out as a function of adsorbent dosage, pH, and contact time. The sorption kinetics and Langmuir and Freundlich isotherms were also studied. Then, the performance of the three materials for phosphate removal were evaluated in flow through column experiments. The originality of the present work lied in the understanding of the relation existing between the physicochemical properties of the adsorbents and their ability to remove phosphate from water. A particular attention was devoted to quantifying the dissolution properties of the minerals (release of Fe^{II}, Al^{III}, Mg^{II}, Ca^{II} in solution) in order to estimate the respective roles of dissolution and adsorption processes in the phosphate removal from water.

2. Materials and methods

2.1. Chemicals

All chemicals used were analytical grade. All experiments were conducted in polypropylene vessels that were soaked in 36% hydrochloric acid (HCl) before use and rinsed with deionized water (Milli-Q, 18.2 $M\Omega\,cm^{-1}$) and ethanol. Deionised water was used for preparing all solutions.

2.2. Adsorbent

Shale, sandstone, and laterite were collected in three regions of Ivory Coast, i.e. shale from the central region (Toumodi (6°28′ N, 4°58′ W)–Lomo North site), sandstone from the southern region (Abidjan (5°21′ N; 4°0′ W)–Akouedo site) and laterite from the eastern region (Abengourou (6°42′ N, 3°28′ W)–Sankadjo site). Sampling was performed in February 2015. Samples were prepared using the same following procedure. Large blocks (diameter of 20 to 30 cm) extracted from the surface soil without any specific tool were first coarsely screened, washed with deionised water to remove the surface-adhered particles and dried in an oven at 50 °C for 24 h. The samples were then crushed again and sieved (AFNOR sieves) to obtain granular sizes of 1–2 mm and $\phi < 400\,\mu m$. Powder samples were finally washed again and dried at 70 °C for 24 h before their use. The main physical characteristics of the three geomaterials obtained for the granular size of 1–2 mm are reported in Table S1. In addition, the chemical composition of the three substrates (Table S2) revealed that all three materials were primarily a mixture of oxides, the major one being SiO_2, Al_2O_3, and Fe_2O_3. The relative amount of these oxides differs from one material to the other. Sandstone was rich in iron, while shale and laterite were Al-rich materials. All three subtrates contained large amounts of Si. The specific surface area of the three powder materials ($\phi < 400\,\mu m$) was determined by multipoint N_2-BET analysis using a Belsorp max surface area analyser (Bel, Japan). The specific surface areas of shale, sandstone, and laterite were 6.3, 28.5, and 37.6 $m^2\,g^{-1}$, respectively.

2.3. Sorption studies

Phosphate sorption onto the three substrates was studied in both batch and column experiments at room temperature. All phosphate concentrations reported in the present study refer to PO_4. A stock phosphate solution (PO_4 250 $mg\,L^{-1}$) of phosphate was prepared by using sodium dihydrogen phosphate ($H_2NaO_4P{\cdot}2H_2O$) and diluted in subsequent experiments.

2.3.1. Batch experiments

The effect of the sorbent dose was examined in a series of experiments that used the same initial phosphate concentration (25 mg $PO_4\,L^{-1}$) while using different adsorbent doses between 0 and 160 $mg\,L^{-1}$. 50-mL flasks were used. The pH of the suspension was maintained at a defined value of 6.5–7.0 by manually adding 0.5 M HCl or 0.5 M NaOH at regular intervals and by using an Almemo 2690 digital pH meter (Ilmenau, Germany) and a WTW glass electrode (Weihleim, Germany). Flasks were capped and stirred magnetically at 300 rpm for 24 h to ensure approximate equilibrium. At the end of this sorption period, 10 mL were withdrawn from the reaction flasks and filtered through 0.22-μm polypropylene syringe filters for phosphorous and aqueous metal species (Ca, Mg, Al, and Fe) analyses by ICP–AES. All experiments were carried out in duplicate to check the reproducibility of the experiments. The pH effect on phosphate removal was examined with a similar procedure using a 25-$mg\,L^{-1}$ initial phosphate concentration and 80 $g\,L^{-1}$ (shale, sandstone and laterite) and 8 $g\,L^{-1}$ (sandstone and laterite) adsorbent dosages while maintaining pH at different values in the range from 2 to 12. Phosphate sorption kinetics were examined in 1-L Erlenmeyer flasks, using an initial phosphate concentration of 25 $mg\,L^{-1}$ and various adsorbent doses for ~60 h. During this reaction period, samples were withdrawn from the flasks at regular intervals of time for phosphate and aqueous metal species determination. The pH of the suspension was maintained at a defined value (6.5–7.0). Sorption isotherm experiments were carried out at pH = 6.5–7.0 in 50-mL Erlenmeyer flasks with varying initial concentrations of phosphate ions (5–

250 mg L^{-1}) and a constant adsorbent dosage of 80 g L^{-1} (shale) and 8 g L^{-1} (sandstone and laterite). The stirring rate was 300 rpm and the equilibration time was 24 h. The phosphate removal efficiency R (%) of the three adsorbents and the phosphate uptake q_t (mg g^{-1}) at time t were calculated from Eqs. (1) and (2), respectively:

$$R = \frac{(C_i - C_t)}{C_i} \times 100 \quad (1)$$

$$q_t = \frac{(C_i - C_t) \times V}{m} \quad (2)$$

where C_i and C_t are the initial phosphate concentration and that at time t, respectively (mg L^{-1}); V is the volume of the solution (L), and m is the mass of material (g). Note that phosphate uptake under near-equilibrium conditions (q_e, mg g^{-1}) is obtained at the equilibrium phosphate concentration $C_t = C_e$.

2.3.2. Column experiments

Plexiglas columns 500 mm in length and with an internal diameter of 37 mm, corresponding to a volume V_{tot} of 473 mL, were used. The columns were packed with dried shale, sandstone or laterite (grain size of 1–2 mm) corresponding to total masses of 593, 661, and 679 g, respectively. Porosity was determined in triplicate by a volumetric method that consisted in determining the volume of water (V_w) required to saturate a known volume of shale (V_s). Porosity (ε) was obtained according to the following formula $\varepsilon = V_w/V_s \times 100$. The porosity of all substrates was very close to 50%; indeed, the porous volume V_P for the three materials was very similar, *i.e.* V_P = 236, 246, and 241 mL for shale, sandstone, and laterite, respectively. An upward-directed water flow was used with the help of a peristaltic pump (Watson-Marlow), ensuring by this way water-saturated conditions. All the columns were first pre-equilibrated with demineralized water during 24 h before performing the phosphate removal experiments. The pH of the phosphate solution ([PO_4] = 25 mg L^{-1}) introduced into the column was close to 5, and the pH measured in the outflow was relatively constant, independently of the nature of the materials used in the columns, with mean pH values of 6.1, 6.0, and 6.4 for shale, sandstone, and laterite, respectively. For both sandstone and laterite columns, a continuous flow of 1 mL min^{-1}, with a corresponding hydraulic retention time (HRT) of ~4 h was used. The total duration of the experiments was ~2.5 months. In order to mimic situations that can be encountered in constructed wetlands where water supply is often provided discontinuously, a water flow circulating discontinuously was used for the shale column, as described in our previous work (Kpannieu et al., 2018). The water flow was 0.23 mL min^{-1} during a first period of 104 h with a corresponding HRT ~ 17 h followed by a shutdown of the water pump corresponding to a HRT of ~ 64 h. The sequence (104 h, 64 h) was repeated nine times for a total duration of the experiments of ~2 months. At appropriate time intervals, 10 mL of solution were sampled in the column outflow and filtered through a 0.22-μm polypropylene syringe filters before phosphate and metal species were analyzed with ICP–AES. The inlet phosphate solution was renewed every two days to limit the bacterial growth.

The phosphate uptake of the column q_{col} (mg g^{-1}), which represented the total amount of adsorbed phosphate on shale, was determined using the following equation:

$$q_{(col)} = \frac{Q}{m} \times \int_0^t (C_0 - C)\mathrm{d}t \quad (3)$$

where Q (L·d^{-1}) is the measured flow rate, m (g) is the mass of the shale in column, C_0 (g·L^{-1}) is the phosphate concentration of the incoming effluent, and C (g L^{-1}) is the phosphate concentration of the outlet effluent.

2.4. Characterization methods

The structural properties of shale, sandstone, and laterite were investigated with X-ray diffraction (XRD) and Mössbauer spectrometry. XRD patterns were acquired with a PANalytical X'Pert Pro Multipurpose diffractometer using Co Kα radiation (λ = 1.78026 Å; 40 kV, 40 mA). Diffraction patterns were obtained over a range of 10–85° 2θ range with a step size of 0.036° and a nominal time per step of 3 s. Transmission Mössbauer spectrometry was performed with a 50-mCi source of ^{57}Co in rhodium to identify and quantify iron phases. The Mössbauer spectra were calibrated relatively to the reference spectrum of a 25 μm thick pure iron foil recorded at room temperature. A cryostat equipped with a closed cycle helium station allows variable temperature measurement between 8 and 300 K. The spectra were fitted using Lorentzian shape lines and, in some cases, Voigt profile analysis, a convolution of a Gaussian distribution with a Lorentzian shape line, was used. Phosphate and metal species (Ca, Mg, Al and Fe) concentrations in solution after syringe filtration were determined by Inductively Coupled Plasma–Atomic Emission Spectrometry (ICP–AES) using an Ultima spectrometer (HORIBA Jobin Yvon).

3. Results and discussion

3.1. Physicochemical properties of the adsorbents

3.1.1. X-ray diffraction (XRD)

All three diffraction patterns (Fig. 1) displayed strong reflection of quartz (SiO_2). Additional reflection lines of silicates minerals such as muscovite ($KAl_2(Si, Al)_4O_{10}(OH)_2$, albite (Na, Ca) $(Si, Al)_4O_8$) and clinochlore $(Mg, Fe)_5(Si_3Al)O_{10}(OH)_8$ were observed for shale, while iron oxides such as goethite (α-FeOOH) and hematite (α-Fe_2O_3) were observed for sandstone and laterite, as already reported (Ngon et al., 2016). Such mineral phases agreed relatively well with the chemical composition reported in Table S2, except as regards the absence of iron-bearing minerals in shale. Because iron is well known to play a key role in phosphate sorption (Altundoğan and Tümen, 2001; Mallet et al., 2013), a closer examination of iron phase minerals contained in the three substrates was carried out using Mössbauer spectrometry.

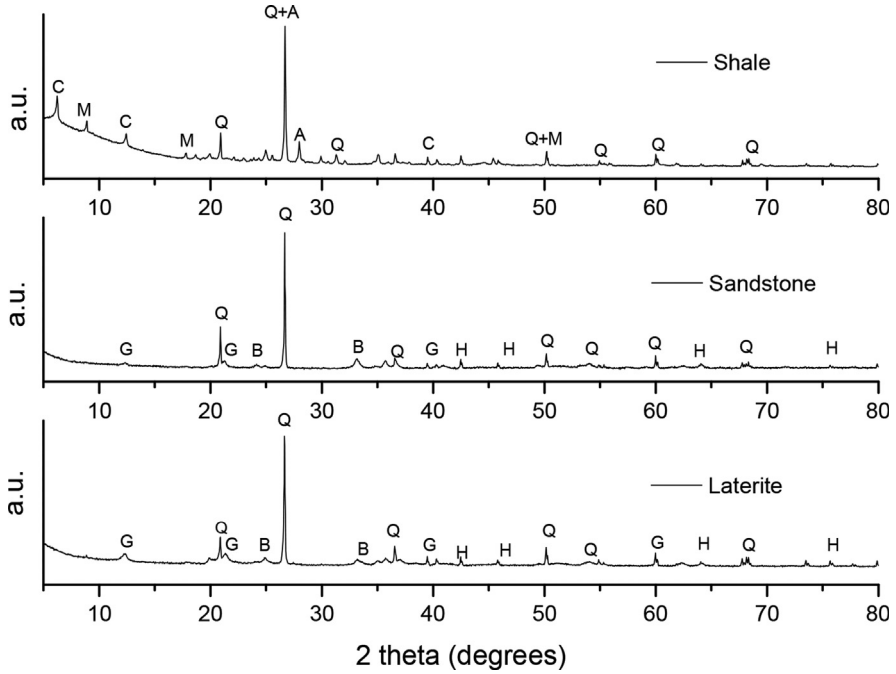

Fig. 1. XRD patterns of naturally occurring shale, sandstone, and laterite from Ivory Coast. The following abbreviations are used: A: albite; B: birnessite; C: clinochlore; G: goethite; H: hematite; M: muscovite, and Q: quartz.

3.1.2. Mössbauer spectrometry

The Mössbauer spectra of sandstone and laterite recorded at room temperature (Fig. 2) exhibit both two magnetic sextets attributed to hematite α-Fe_2O_3 and goethite α-FeOOH (Fritsch et al., 2011) and a ferric paramagnetic doublet D_1 (Table S3), in agreement with XRD analyses. Mössbauer analysis at lower temperature was needed to distinguish whether the paramagnetic doublet D_1 recorded at room temperature corresponded to iron oxides or to Fe^{III} species embedded in the structure of

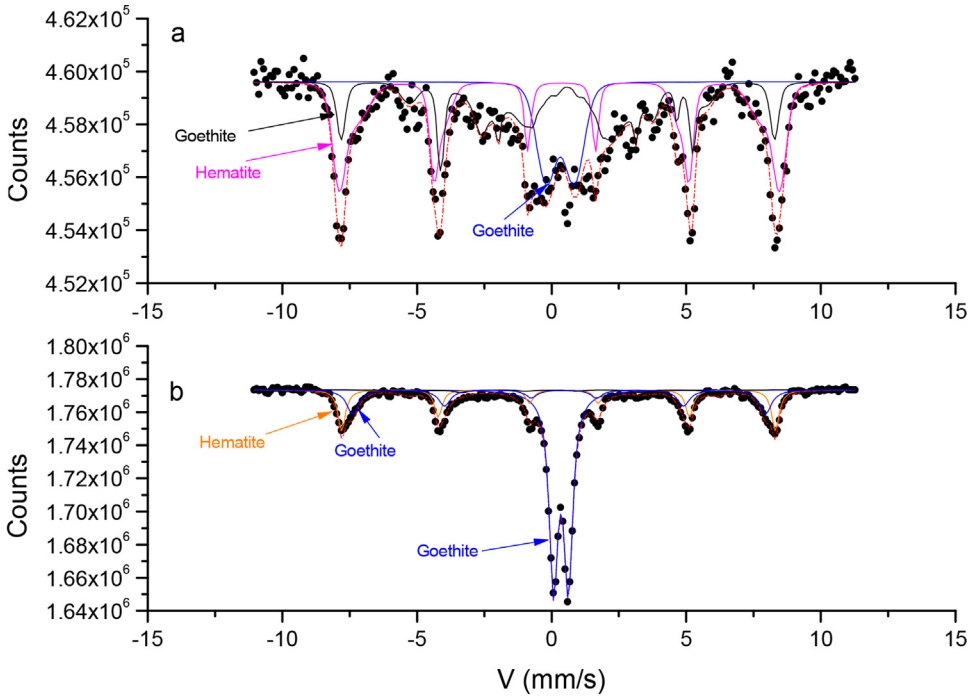

Fig. 2. Mössbauer spectra of naturally occurring sandstone (a) and laterite (b) from Ivory Coast at room temperature.

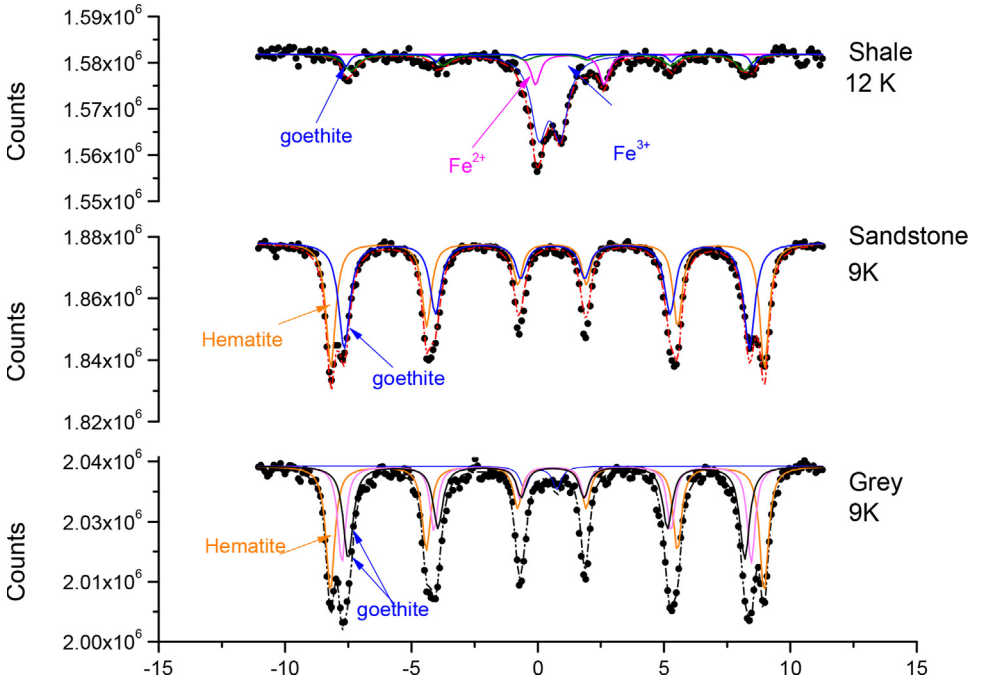

Fig. 3. Mössbauer spectra of naturally occurring shale, sandstone and laterite from Ivory Coast at 12 K (shale) and 9 K (sandstone and laterite).

clays. The Mössbauer spectra of sandstone and laterite recorded at 9 K (Fig. 3) clearly showed that the doublet observed at 300 K has been transformed into a magnetic sextet attributed to α-FeOOH (Kone et al., 2009). The corresponding Mössbauer hyperfine parameters (Table S4) revealed that only a very low intensity (RA of ~ 3%) paramagnetic doublet remained on the 9 K Mössbauer spectrum of laterite and could be attributed to structural Fe^{III} species into clays. Therefore, for both sandstone and laterite, Fe^{III} species were essentially included into ferric oxides (α-Fe_2O_3 and α-FeOOH), and the ferric doublet recorded at room temperature (Fig. 2) was attributed to superparamagnetic goethite (Janot et al., 1973). This means that the size of some of the goethite particles in sandstone and laterite is quite small. This must be particularly true for laterite, since the ferric doublet recorded at room temperature is relatively intense (RA of ~ 55%) and narrow and does not exhibit any relaxation effect (Table S3). This last result may be cautiously correlated to the BET analysis showing that laterite and sandstone had the highest surface specific area, although the materials were composed of a mixture of minerals. In fact, it can be hypothesized that the presence of small iron particles in laterite and sandstone contribute to a global increase of the specific surface area. The status of iron in shale was very different, and the Mössbauer spectrum recorded at 12 K (Fig. 3) exhibits a ferric (D_1) and a ferrous (D_2) paramagnetic doublet. The total relative areas of both doublets are relatively high, representing ~ 2/3 of the total spectra. This means that, for the shale, most of the iron species was embedded in the clay minerals (muscovite, clinochlore), contrary to sandstone and laterite, where iron was present in iron oxides. However, the shale did also contain some iron in goethite, as shown by the magnetic sextet of α-FeOOH observed at 12 K (Fig. 3).

3.2. Phosphate sorption in batch experiments

3.2.1. Effect of adsorbent dosage

All three substrates displayed not surprisingly an increase in the removal efficiency with increasing adsorbent dosage (Fig. 4). A high removal efficiency of 100% was achieved with laterite and sandstone at 20 and 40 g L^{-1}, respectively, while the removal efficiency remained less than 100% in the whole sorbent dose studied for shale (Fig. 4a). In addition, the phosphate uptake strongly decreased as the dosage increased and reached a saturation level at high sorbent doses (Fig. 4b). Such results reflected that adsorbed phosphate species were distributed among more available sorption sites at high sorbent doses, thus decreasing the sorption capacity (Ádám et al., 2007; Babatunde et al., 2009).

3.2.2. Effect of pH on phosphate removal sorption

The pH is an important factor that strongly influences the phosphate sorption mechanisms at the solid–solution interfaces. Small amounts of phosphate are determined at pH values lower than 8 and 10 for sandstone and laterite, respectively, which indicated a phosphate removal efficiency close to 100% (Fig. 5). Beyond these two pH values, phosphate concentration strongly increased. A different behavior was observed for shale. In fact, an increase in phosphate concentration was observed in the pH range of 2–11, followed by a strong decrease beyond pH 11. The inset in Fig. 5 displays the phosphate concentration determined in solution for a laterite and sandstone dosage

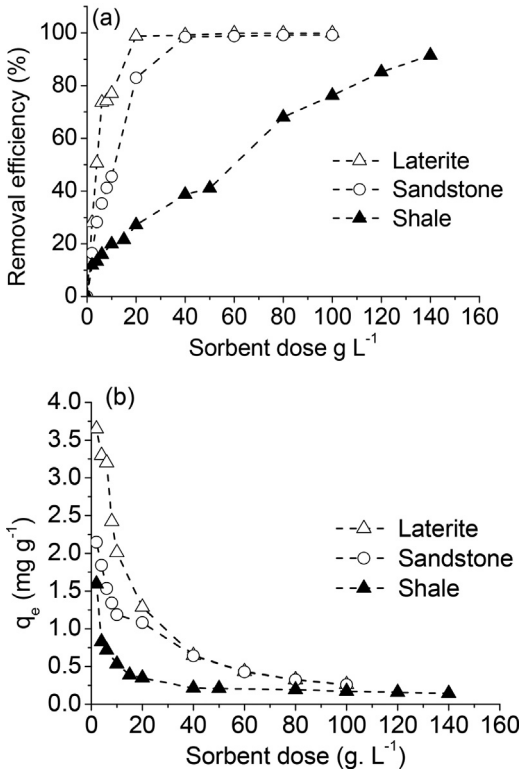

Fig. 4. Phosphate removal (a) and phosphate uptake (b) for shale, sandstone, and laterite as a function of the dose of adsorbent ($[PO_4]_{initial}$ = 25 mg L^{-1}; time contact: 24 h).

of 8 g L^{-1}. The phosphate concentration increased over the whole pH range studied. It can thus be concluded that increasing the pH resulted in a decrease of the phosphate removal efficiency (at phosphate removal efficiencies lower than 100%), except for shale, for which a stronger removal efficiency was observed at pH 12. With the exception of this high pH value, the phosphate removal efficiency of shale was much smaller than those for sandstone and laterite.

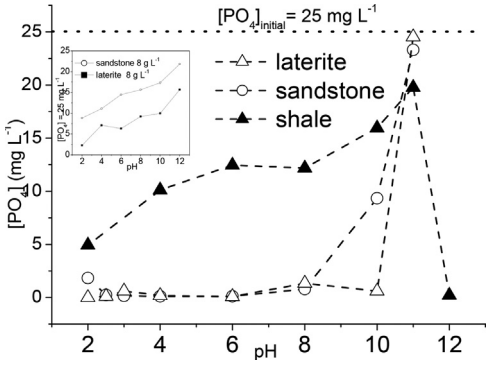

Fig. 5. Aqueous phosphate concentration as a function of pH after sandstone, laterite and shale reaction with a 25mg L^{-1} initial phosphate solution ([sorbent] = 80 g L^{-1} and 8 g L^{-1} (inset); time contact: 24 h).

3.2.3. Ions concentration as a function of pH

To further investigate the phosphate removal mechanism, aqueous ions release was studied as a function of pH in blank (without phosphate) and after adsorbents reaction with a 25mg L^{-1} phosphate solution (Fig. 6 and supplementary Figure S1). Blank experiments revealed, in the low pH range, a strong release of Ca, Mg and Al, and to a lesser extent Fe species for shale, compared to sandstone and laterite. Dissolution processes without added phosphate are thus much more pronounced for shale in acidic conditions. Moreover, sandstone and laterite clearly exhibited a behavior towards phosphate sorption different from that of shale. In fact, low amounts of Ca, Mg, Al, and Fe were determined in solution after shale reaction with phosphate ions and whatever the pH was (Fig. 6). Additionally, calcium and magnesium concentrations did not significantly differ in blank experiments and after phosphate reaction with sandstone and laterite, even at a lower dosage of 8 g L^{-1} (data not shown). Some differences in ion concentrations were observed at low pH, where the presence of phosphate ions induced an increase in Fe and Al dissolution processes in laterite and sandstone, respectively. From Figs. 5 and 6, it clearly appears that shale displayed a different sorption behavior from those of sandstone and laterite. The weak dissolution processes on phosphate removal in the case of sandstone and laterite combined to a much more efficient phosphate removal clearly suggested that phosphate sorption was dominated by adsorption processes. Adsorption processes controlled phosphate sorption in a pH range of 4–11 for shale, but dissolution of shale followed by precipitation of the released aqueous species with phosphate competes with adsorption under low pH conditions (Kpannieu et al., 2018).

3.2.4. Phosphate sorption kinetics

Sorption kinetics were obtained with 80 g L^{-1} (shale) and 8 g L^{-1} (laterite and sandstone) sorbent doses (Fig. 7). The results obtained at additional sorbent doses for laterite and sandstone are displayed as supporting information (Supplementary Figures S2 and S3). All curves displayed almost the same shape. The sorption rate was rapid at the beginning of the experiments, and then decreased until a pseudo-plateau was reached. The first step may be due to phosphate sorption at the external surface of the sorbents, while the second step probably reflected some slow sorption process due to phosphate diffusion into the pores of the sorbent (Sanyal and De Datta, 1991; Yang et al., 2006). The phosphate uptake decreased in the following order: laterite > sandstone > shale. In particular, the observed maximal phosphate uptakes determined from Fig. 7 were 3.2, 2.8, and 0.23 mg g^{-1} for laterite, sandstone, and shale, respectively. The sorption capacity of shale was thus smaller than those of laterite and sandstone by more than a factor of 10. Common pseudo-first-order and pseudo-second-order equations were used to model the experimental data using a linear fit approach (Eqs. (4) and (5)):

- pseudo-first-order equation:

$$\log(q_e - q_t) = \log q_e - \frac{k_1 t}{2.303} \quad (4)$$

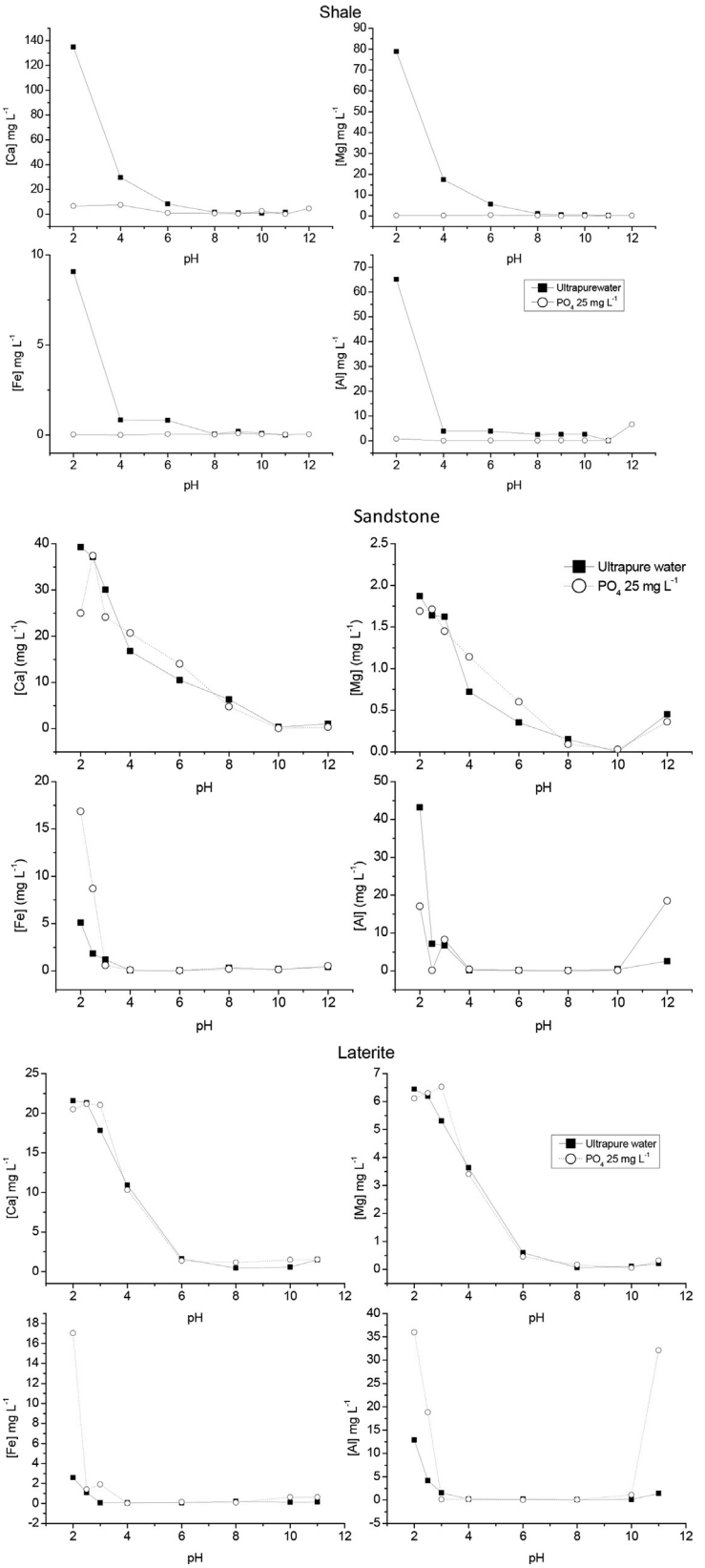

Fig. 6. Ion concentrations in solution in blank experiments (without PO_4) and after reaction with a 25mg L^{-1} initial phosphate solution ([sorbent] = 80 g L^{-1}; pH ~ 7; time contact: 24 h).

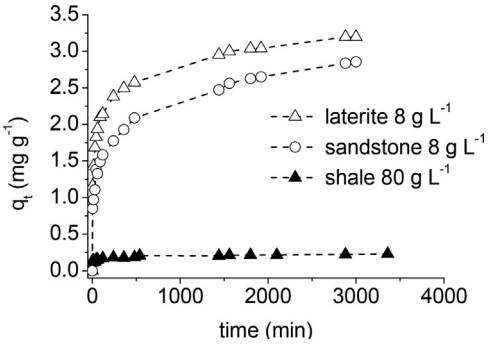

Fig. 7. Effect of contact time on phosphate uptake capacity by sandstone, laterite, and shale ($[PO_4]_{initial}$ = 25 mg L^{-1}; pH ~ 7; contact time: 24 h).

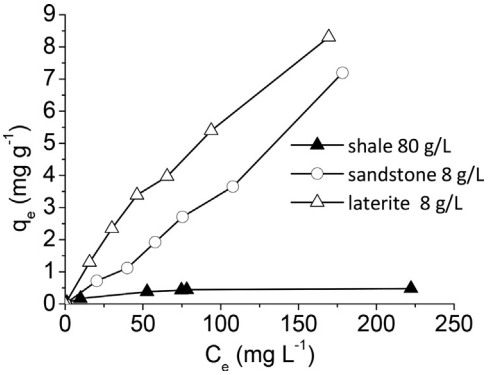

Fig. 8. Adsorption isotherms of phosphate for the three different sorbents (pH ~ 7; time contact: 24 h). The dashed line is only drawn as a visual help.

• pseudo-second-order equation:

$$\frac{t}{q_t} = \frac{1}{k_2\ q_e^2} + \frac{t}{q_e} \quad (5)$$

where q_e (mg g^{-1}) is the equilibrium sorption amount, q_t (mg g^{-1}) is the amount of phosphate adsorbed at any time t and k_1 (min^{-1}) and k_2 (g mg^{-1} min^{-1}) are the pseudo-first-order and pseudo-second-order rate constants, respectively.

The linear plots of phosphate sorption kinetics obtained and the corresponding kinetic parameters are given in Supplementary Figures S4 and S5, and Table S5 respectively. The kinetic data could only be well described using the pseudo-second-order kinetic model. High correlation coefficients were in fact obtained and the equilibrium sorption amounts (q_{cal}) closely match the experimental data, while the pseudo first-order-model did not fit the data.

Similar kinetics results were reported in the literature for various phosphate adsorbents (Cai et al., 2012; Namasivayam and Prathap, 2005; Zhu et al., 2009). Such results indicated that the sorption process of phosphate on these three materials may be based on chemisorption. As the sorbent dose increased and the other experimental conditions remained unchanged, the value of k_2 increased by a factor higher than 10.

3.2.5. Phosphate sorption isotherms

Isotherms are commonly used to describe the sorption behavior of a given adsorbent (Liu and Zhang, 2015; Yang et al., 2014). The sorption behavior of laterite and sandstone was clearly different from that of shale (Fig. 8). As it is the case in most studies, the shale curve displayed a saturation point at which increasing the initial phosphate concentration did not cause a significant increase in the phosphate sorption capacity (Zhu et al., 2009). The presence of this saturation level allowed us to fit the data by using the common Langmuir and Freundlich models (S). The obtained parameters for both Langmuir and Freundlich models are reported in Supplementary Table S6. The data were better fitted by using the Langmuir model. The Langmuir linear plot of shale is displayed in Supplementary Figure S6. Isotherms obtained for laterite and sandstone did not display any saturation level, which made the prediction of the sorption capacity unreliable. A careful examination of the data suggested that sandstone and laterite isotherms are close to C-type isotherms (Limousin et al., 2007). In fact, coefficient correlations of 0.989 and 0.988 were obtained for sandstone and laterite, respectively, by using a linear data fitting approach (data not shown). Such a behavior has already been reported in the literature for phosphate sorption by substrates used in constructed wetlands and phosphate retention in filter materials such as shellsand and filtralite P® (Boeykens et al., 2017; Drizo et al., 1999). In any way, the maximum phosphate uptake varied between 0.48 for shale and 8.3 mg g^{-1} for laterite. Note that the shale dose was ten times higher than those of sandstone and laterite. The uptake capacities of laterite were higher than those reported for other natural minerals such as bauxite (0.6 mg g^{-1}) (Drizo et al., 1999), limestone (0.55 mg g^{-1}) (Drizo et al., 1999), zeolite (0.25 mg g^{-1}) (Drizo et al., 1999), dolomite (0.3 mg g^{-1}) (Pant et al., 2001), and apatite (0.41 mg g^{-1}) (Bellier et al., 2006). Additionally, all these literature data were obtained at higher initial phosphate concentrations (40–150 mg L^{-1}). The ranking order of the maximum sorption capacity was therefore again: laterite > sandstone > shale. Remind that the specific surface areas of shale, sandstone, and laterite were 6.3, 28.5, and 37.6 m^2 g^{-1}, respectively. It thus appeared that the material with the lowest specific surface area had the lowest phosphate uptake capacity. One reason for this may be that phosphate sorption was decreased by limited available surface sorption sites in the case of shale. Another reason explaining the lowest capacity of shale for phosphate removal was the status of iron. Indeed, the shale contained the lowest quantity of iron (Table S2) and the lowest proportion of Fe in iron oxides, *i.e.* 31% compared with 97% and 100% observed for laterite and sandstone, respectively. Iron oxide particles, in particular those with low crystal size, are well known to develop strong bonding sites for surface complexation by phosphate species. The superiority of laterite for phosphate removal in comparison with

shale and sandstone may be correlated to the existence of goethite particles with very low crystal size, as testified by the superparamagnetic behaviour observed for this mineral at room temperature by Mössbauer spectroscopy. Interestingly, sorption capacities were recalculated by taking into account the specific surface area of laterite and sandstone; similar values close to 0.2 mg m^{-2} were obtained, thus suggesting that the difference in reactivity was due to a particle size effect, in agreement with Mössbauer analysis.

3.3. Phosphate sorption in hydrodynamic conditions: column tests

The breakthrough curves of sandstone and laterite obtained at a flow rate of 1 mL min^{-1} and a corresponding HRT of ~4 h are displayed in Fig. 9. We noticed that the breakthrough curve of laterite presented an unsual shape, with two plateaus. The origin of this behaviour was outside the scope of the present study. As expected from the batch experiments, the breakthrough observed for laterite occurred later than the one observed for sandstone. Indeed, if a threshold of $[PO_4] = 1$ mg L^{-1} was chosen, *i.e.* a C/C_0 of 0.04 with $C_0 = 25$ mg L^{-1}, the breakthrough occurred at a value of V/V_P of ~147 and 132 for laterite and sandstone, respectively. These values were about 8 times higher than the breakthrough observed previously for shale, *i.e.* $V/V_P \sim 17$, even though the mean HRT of ~35 h used for shale was much higher than the one used for sandstone and laterite. Therefore, the column experiments confirmed that the capacity of shale to remove phosphate was the lowest, as already observed in batch experiments. The removal capacity at the breakthrough q_{break} can be computed as $q_{break} = 0.17$, 1.23, and 1.30 mg PO_4 g^{-1} for shale, sandstone, and laterite, respectively. Calcium, magnesium, and phosphate ions concentrations are displayed as a function of time (Fig. 10). The initial calcium (4.9 and 9.2 mg L^{-1} for laterite and sandstone, respectively), magnesium (1.8 and 1 mg L^{-1}), aluminum (not detected) and iron (not detected) concentrations in the outflow were in good agreement with the equilibrium data recorded at a pH of 5 in batch experiments. The soluble calcium and magnesium concentrations in the outflow decreased continuously and

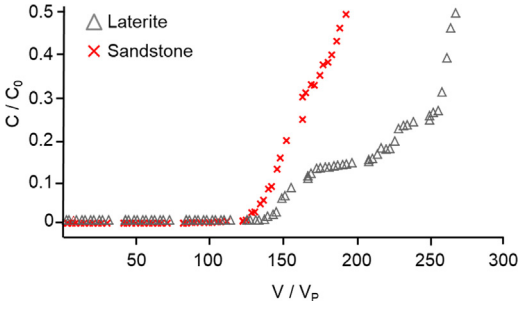

Fig. 9. Breakthrough curves obtained for the sandstone and laterite column experiments in hydrodynamic conditions (flow of 1 mL min^{-1}, $C_0 = 25$ mg PO_4 L^{-1}).

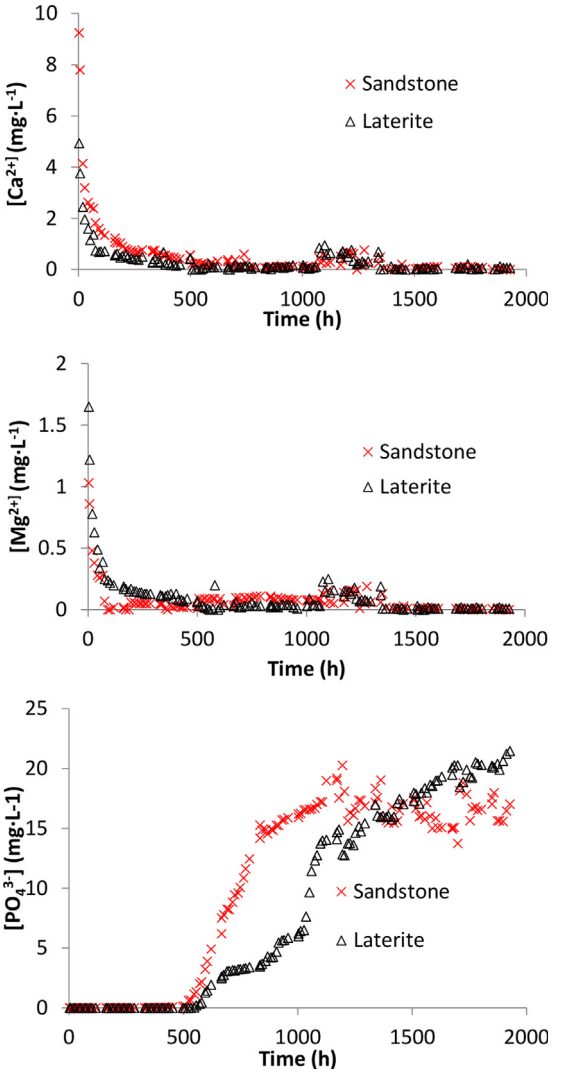

Fig. 10. Ca^{2+}, Mg^{2+}, and PO_4^{3-} concentrations as a function of time in sandstone and laterite column experiments in hydrodynamic conditions (ϕ 1–2 mm).

reached a value lower than 0.5 mg L^{-1} at the breakthrough. Experiments carried out in hydrodynamic mode required a preliminary step in which the column was pre-equilibrated with ultra-pure water during 24 h before the phosphate solution flowed through the column. The aqueous species concentrations determined at $t = 0$ thus reflected the equilibria solubility that occurred during this period (Fig. 10). In this experimental situation, phosphate removal partially occurred through reaction with the soluble species released in solution during the column equilibration. In fact, a correlation between the decrease in Ca and Mg concentrations and the increase in phosphate concentration at the outflow of the column was evidenced. Iron concentration as a function of time remained below the detection limit (data not shown). Such behavior had already been reported in the literature for shellsand and

filtralite P® filter materials (Ádám et al., 2007). According to this study, phosphate removal occurred through the accumulation of large amounts of Ca (45–260 mg L^{-1}) and Mg ions (5–65 mg L^{-1}) at the beginning of the column experiment. The removal capacity at the breakthrough measured for filtralite P® and shellsand can be calculated from the data provided in this previous work (Ádám et al., 2007) and was evaluated to be respectively ~0.6 and 0.9 mg PO_4 g^{-1} for a contact time of ~4 days. Therefore, the removal capacity of laterite and sandstone from Ivory Coast was at least of the same order of magnitude than the one reported for the shellsand from Hordaland Tørkeri in Norway, which was recognized as a very efficient granular natural material for phosphate removal in hydrodynamic conditions.

4. Conclusion

The removal of phosphate by three natural materials from Ivory Coast was studied in homogeneous batch suspensions and in static/hydrodynamic conditions in column experiments. Interestingly, the three geomaterials exhibit different sorption behaviors: phosphate removal is dominated by adsorption for laterite and sandstone, while dissolution processes may compete for adsorption at low pH for shale. The investigations revealed that all three materials retained phosphate to various extents. Batch experiments showed that the most efficient phosphate adsorbent was laterite, followed by sandstone and shale, the sorption efficiency of shale being strongly smaller than those of laterite and sandstone. The removal of phosphate by adsorption on iron oxides was certainly very limited in shale studied here, since most of the iron species were situated in structural substitution into the bulk of the solid clay minerals. In contrast most of the iron in laterite and sandstone occurred as separate iron oxides minerals (goethite and hematite). Laterite was also the most efficient mineral for removing phosphate in flow through conditions with a phosphate removal capacity at the breakthrough higher than 1 mg PO_4 g^{-1}. Therefore, laterite is a very promising mineral and may be considered for phosphate removal at a larger scale, *i.e.* in a micro-pilot unit before ultimately being tested in wetlands in Ivory Coast.

Acknowledgements

The authors thank G. Medjahdi (Centre of X-gamma Competence; UMR 7198 CNRS–Université de Lorraine, Nancy, France) for XRD analyses, and C. Genois from the LCPME is gratefully acknowledged for ICP analyses.

Appendix A. Supplementary data

Supplementary data associated with this article can be found, in the online version, at https://doi.org/10.1016/j.crte.2018.09.004.

References

Ádám, K., Krogstad, T., Vråle, L., Søvik, A.K., Jenssen, P.D., 2007. Phosphorus retention in the filter materials shellsand and filtralite P®—Batch and column experiment with synthetic P solution and secondary wastewater. Ecol. Engin. 29, 200–208.

Altundoğan, H.S., Tümen, F., 2001. Removal of phosphates from aqueous solutions by using bauxite. I: Effect of pH on the adsorption of various phosphates. J. Chem. Technol. Biotechnol. 77, 77–85.

Babatunde, A.O., Zhao, Y.Q., Burke, A.M., Morris, M.A., Hanrahan, J.P., 2009. Characterization of aluminium-based water treatment residual for potential phosphorus removal in engineered wetlands. Environ. Pollut. 157, 2830–2836.

Bellier, N., Chazarenc, F., Comeau, Y., 2006. Phosphorus removal from wastewater by mineral apatite. Water Res. 40 (15), 2965–2971.

Boeykens, S.P., Piol, M., Legal, N., Saralegui, L.S., Vazquez, A.B.C., 2017. Eutrophication decrease: phosphate adsorption processes in presence of nitrates. J. Environ. Manage. 203, 888–895.

Boyer, T.H., Persaud, A., Banerjee, P., Palomino, P., 2011. Comparison of low-cost and engineered materials for phosphorus removal from organic-rich surface water. Water Res. 45, 4803–4814.

Briton Bi, G.H., Yao, B., Ado, G., 2007. Evaluation of the Abidjan lagoon pollution. J. Appl. Sci. Environ. Manage. 11 (2), 173–179.

Cai, P., Zheng, H., Wang, C., Ma, H., Hu, J., Pu, Y., Liang, P., 2012. Competitive adsorption characteristics of fluoride and phosphate on calcinated Mg-Al-CO_3 layered double hydroxides. J. Hazard. Mat. 213–214, 100–108.

Drizo, A., Frost, C.A., Grace, J., Smith, K.A., 1999. Physicochemical screening of phosphate-removing substrates for use in constructed wetland systems. Water Res. 33, 595–3602.

Fritsch, E., Balan, E., Nascimento, N.D.R., Allard, T., Bardy, M., Bueno, G., Derenne, S., Melfi, A.J., Calas, G., 2011. Deciphering the weathering processes using environmental mineralogy and geochemistry: towards an integrated model of laterite and podzol genesis in the Upper Amazon Basin. C. R. Geoscience 343, 188–198.

Hongbin, Y., Ming, K., 2014. Simultaneous removal of ammonium and phosphate from eutrophic waters using natural calcium-rich attapulgite-based versatile adsorbent. Desalination 351, 128–137.

Janot, C., Gibert, H., Tobias, C., 1973. Caracterisation de kaolinites ferrifères par spectrométrie Mössbauer. Bull. Soc. Fr. Mineral. Cristallogr. 96, 281–291.

Johansson-Westholm, L., 2006. Review—Substrates for phosphorus removal—Potential benefits for on-site wastewater treatment? Water Res. 40 (1), 23–36.

Koffi, S.O., Coffy, A.A., Villeneuve, J.P., Sess, D.E., N'Guessan, Y.T., 2009. Pollution of a tropical lagoon by the determination of organochlorine coumpounds. Tropicultura 27 (2), 77–82.

Kone, T., Hanna, K., Abdelmoula, M., Ruby, C., Carteret, C., 2009. Reductive transformation and mineralization of an azo dye by hydroxysulphate green rust preceding oxidation using H_2O_2 at neutral pH. Chemosphere 75, 212–219.

Kpannieu, D.E., Ruby, C., Coulibaly, L., Abdelmoula, M., Mallet, M., 2018. Removal of phosphate by shale from Ivory Coast in homogeneous reactor and hydrodynamic conditions: influence of soluble species. Clays Clays Min. (in press).

Limousin, G., Goudet, J.-P., Charlet, L., Szenknect, S., Barthès, V., Krimissa, M., 2007. Sorption isotherms: a review on physical bases, modeling and measurement. Appl. Geochem. 22, 249–275.

Liu, X., Zhang, L., 2015. Removal of phosphate anions using the modified chitosan beads: adsorption kinetic, isotherm and mechanism studies. Powder Technol. 277, 112–119.

Mallet, M., Barthélémy, K., Ruby, C., Renard, A., Naille, S., 2013. Investigation of phosphate adsorption onto ferrihydrite by X-ray Photoelectron Spectroscopy. J. Colloid Interf. Sci. 407, 95–101.

Namasivayam, C., Prathap, K., 2005. Recycling Fe(III)/Cr(III) hydroxide, an industrial solid waste for the removal of phosphate from water. J. Hazard. Mat. 123 (1–3), 127–134.

Ngon, G.F., Etame, J., Ntamak-Nida, M.J., Mbesse, C.O., Mbai, J.S., Bayiga, E.C., Gerard, M., 2016. Geochemical and palaeoenvironmental characteristics of Missole I iron duricrusts of the Douala sub-basin (Western Cameroon). C. R. Geoscience 348, 127–137.

Pant, H.K., Reddy, K.R., Lemon, E., 2001. Phosphorus retention capacity of root bed media of subsurface flow constructed wetlands. Ecol. Eng. 17, 345–355.

Sanyal, S.K., De Datta, S.K., 1991. Chemistry of phosphorus transformation in soils. Adv. Soil Sci. 16, 1–94.

Tuo, A.D., Soro, M.B., Trokourey, A., Bokra, Y., 2012. Assessment of waters contamination by nutrients and heavy metals in the Ebrie Lagoon (Abidjan, Ivory Coast). Res. J. Environ. Toxicol. 6 (5), 198–209.

Vohla, C., Kõiv, M., Bavor, H.J., Chazarenc, F., Mander, Ü., 2011. Filter materials for phosphorus removal from wastewater in treatment wetlands–A review. Ecol. Eng. 37 (1), 70–89.

Wendling, L.A., Douglas, G.B., Coleman, S., Yuan, Z., 2013. Nutrient and dissolved organic carbon removal from natural waters using industrial by-products. Sci. Total Environ. 442, 63–72.

Yang, Y., Tomlinson, D., Kennedy, S., Zhao, Y.Q., 2006. Dewatered alum sludge: a potential adsorbent for phosphorus removal. Wat. Sci. Tech. 54 (5), 207–213.

Yang, M., Lina, J., Zhana, Y., Zhang, H., 2014. Adsorption of phosphate from water on lake sediments amended with zirconium-modified zeolites in batch mode. Ecol. Eng. 71, 223–233.

Yao, K.M., Metongo, B.S., Trokourey, A., Bokra, Y., 2009. La pollution des eaux de la zone urbaine d'une lagune tropicale par les matières oxydables (lagune Ebrié, Côte d'Ivoire). Int. J. Chem. Sci. 3 (4), 755–770.

Zhu, M.X., Ding, K.Y., Xu, S.H., Jiang, X., 2009. Adsorption of phosphate on hydroxyaluminum-and hydroxyiron-montmorillonite complexes. J. Hazard. Mat. 165, 645–651.